Origins of Dry Air in the Tropics and Subtropics

PIERO CAU, JOHN METHVEN, AND BRIAN HOSKINS

Department of Meteorology, University of Reading, Reading, United Kingdom

(Manuscript received 16 May 2006, in final form 19 September 2006)

ABSTRACT

The humidity in the dry regions of the tropical and subtropical troposphere has a major impact on the ability of the atmosphere to radiate heat to space. The water vapor content in these regions is determined by their "origins," here defined as the last condensation event following air masses. Trajectory simulations are used to investigate such origins using the 40-yr European Centre for Medium-Range Weather Forecasts Re-Analysis (ERA-40) data for January 1993. It is shown that 96% of air parcels experience condensation within 24 days and most of the remaining 4% originate in the stratosphere. Dry air masses are shown to experience a net pressure increase since last condensation, which is uniform with latitude, while the median time taken for descent is 5 days into the subtropics but exceeds 16 days into the equatorial lower troposphere. The associated rate of decrease in potential temperature is consistent with radiative cooling. The relationship between the drier regions in the Tropics and subtropics and the geographical localization of their origin is investigated. Four transport processes are identified to explain these relationships.

1. Introduction

The dry regions of the tropical and subtropical troposphere have a significant impact on the water vapor feedback and the atmospheric response to increased anthropogenic gases (Houghton et al. 2001). The relative transparency of a layer of dry air (20% relative humidity) inserted into the average tropical humidity profile was shown by Cau et al. (2005) to lead to an increase in outgoing longwave radiation of about 3 $\mathrm{W\,m^{-2}}$ $(100\ \mathrm{hPa})^{-1}$ thickness in a clear-sky scenario, approximately independent of layer altitude. Such sensitivity implies that the distribution of humidity can have a significant role in the response of the Tropics in a climate-change scenario.

Since specific humidity is conserved following an air mass in the absence of phase changes or mixing, its humidity is determined at the instant when condensation last occurred (assuming weak mixing and that the reevaporation of condensate is not important). The mixing ratio set by the condensation event depends on pressure as well as the saturation vapor pressure in that location and on critical relative humidity for condensation (which may exceed 100% with respect to ice). Therefore, changes to the temperature distribution (in pressure coordinates) will alter the humidity distribution. The impact is nonlocal since a dry air mass can only achieve low relative humidity (<20%) by moving to a location where the saturation mixing ratio is much higher than at its origin defined by the last condensation event. Typically, this subsaturation is attained by descent and the associated adiabatic warming is implied. Of course, the humidity distribution could also change if the temperature distribution were unaltered, but trajectories alter because of circulation pattern changes. Therefore, the links between regions of saturation and the dryness of the Tropics and the subtropics need to be understood. In this paper, the distribution and origins of dry air masses are examined within the Tropics and the subtropics (spanning 40°N–40°S) during January 1993.

The distribution of humidity in the troposphere depends on several different processes, occurring over a very broad range of scales. They include large-scale advection (Pierrehumbert and Roca 1998), turbulent transport associated with convection (Soden and Fu 1995), advection and evaporation of cloud condensates and precipitation (Sun and Lindzen 1993), and the microphysics of condensation into the ice phase. Despite the potential complexity, a number of recent studies (Sherwood 1996; Salathé and Hartmann 1997; Pierre-

Corresponding author address: John Methven, Dept. of Meteorology, University of Reading, P.O. Box 243, Earley Gate, Reading, RG6 6BB, United Kingdom.
E-mail: j.methven@reading.ac.uk

DOI: 10.1175/JCLI4176.1

humbert and Roca 1998; Pierrehumbert 1999; Cau et al. 2005; Sherwood et al. 2006) have shown that tropospheric humidity can be understood to first order by considering advection and saturation alone. This can be attributed to the long intervals (many days) that can occur between humidity-setting events, making specific humidity a good tracer, although we will show in section 2b that the effects of remoistening following air masses cannot be ignored. Long-lived tracer structures are stretched and folded by the large-scale winds, resulting in a cascade toward smaller scales. Consequently, Lagrangian simulations of tracers are accurate for structures with widths at least 6 times smaller than the resolution of the analyzed winds (Methven and Hoskins 1999). These conclusions were based on idealized baroclinic life cycle experiments and stratospheric analyses but have been supported in simulations of aircraft measurements in the extratropical troposphere (Methven et al. 2003). Cau et al. (2005) extended this evidence to the Tropics by simulating humidity profiles observed by high-resolution radiosondes launched during the Tropical Ocean Global Atmosphere Coupled Ocean–Atmosphere Response Experiment (TOGA COARE) observation period in 1992–93. All observed dry layers with thicknesses exceeding 50 hPa were captured in trajectory simulations.

In this paper, trajectory techniques are used to calculate the origins of dry air masses. A similar approach was used by Salathé and Hartmann (1997), who focused on the tropical upper-tropospheric humidity and used horizontal backward trajectories from dry regions into convective regions to establish the sources of dry air. They concluded that radiatively driven subsidence along air trajectories appears to govern the decrease in upper-tropospheric relative humidity in the outflow of tropical convection and that horizontal moisture transport can reproduce the observed moisture distribution in the Tropics provided accurate observation of convection and horizontal winds are available.

More recently, Galewsky et al. (2005) have devised a technique for diagnosing the mechanisms that control the humidity in a general circulation model (GCM) and in reanalysis data. The atmosphere is divided into a large set of subdomains, each of which is associated with a tracer (defined on the GCM grid) that tracks the air that was last saturated there. If saturation occurs in one of the grid cells that belongs to a given subdomain, the value of the corresponding tracer is set to 1 in that cell while all tracers associated with other subdomains are set to 0 on that same cell. Such tracers are simply advected by the large-scale flow and their value in each grid cell at any given time corresponds to the probability of the associated subdomain being where air experienced the last condensation event. Comparing the values of all tracers in a given cell, it is then possible to estimate the contribution of each subdomain to the humidity on that cell. They used this technique both with a general circulation model and the National Centers for Environmental Prediction–National Center for Atmospheric Research (NCEP–NCAR) reanalysis data for winter [December–February (DJF)] 2001–02 to investigate the subtropical humidity dynamics. They found that diabatic descent from the tropical upper troposphere plays a secondary role in controlling the dryness of the subtropics. Instead they found that air descending adiabatically is likely to get caught up in midlatitude eddies that bring it upward and poleward along isentropes, saturate it at low temperature, and then return it dehydrated into the subtropics.

This paper will begin by focusing on the identification of condensation events using trajectories and humidity analyses and the statistics of time elapsed since the last condensation. The results are specific to the origin of humidity and differ from "tracer age," which is usually defined as the elapsed time since an air mass was last in contact with a particular control surface (such as the tropopause in the case of stratospheric tracer age; Holzer and Hall 2000). The sensitivity to assumptions about critical relative humidity for condensation are also explored.

In section 3, the Lagrangian mean changes in pressure and potential temperature since the last condensation are found for air masses arriving dry in the Tropics and subtropics. The picture is then expanded in section 4 by dividing the domain into three pressure layers and three latitude bands and considering the Lagrangian mean motion in the meridional plane. In section 5, the relationships between dry regions and their origins are projected onto the horizontal plane. Commonalities in trajectory behavior linking the humidity origins to dry regions are synthesized in terms of four distinct transport mechanisms. Conclusions are drawn in section 6.

2. Time since last condensation (τ)

a. Back trajectory calculations

Twenty-four-day back trajectories were "released" daily from a grid covering all of the Tropics and the subtropics from 38°N to 38°S. The grid was regular in longitude (λ), the sine of latitude ($\mu = \sin\phi$), and pressure (p) so that the fraction of trajectories with a particular behavior approximates the fraction of mass. There were 90 grid points in λ, 19 grid points in μ, and the pressure spacing was 50 hPa ranging from 975 to 175 hPa. In the following discussion this grid will be

referred to as the "arrival grid" for air masses present at the analysis time.

The trajectories were calculated using the U.K. Universities Global Atmospheric Modeling Programme (UGAMP) trajectory code (Methven 1997) driven by the European Centre for Medium-Range Weather Forecasts (ECMWF) analyses, which have been shown to be capable of simulating accurately almost all dry air mass structures in the extratropics with widths above 30 km (Methven and Hoskins 1999; Methven et al. 2003) and the occurrence of all dry layers thicker than 50 hPa observed in the Tropics during TOGA COARE (Cau et al. 2005). In this paper, January 1993 is investigated because the performance of the trajectory code has been evaluated for this season using high-resolution radiosonde ascents from the tropical TOGA COARE network. The UGAMP trajectory model has also been used to examine the transport of air across the tropical tropopause layer into the stratosphere (Jackson et al. 2001; Bonazzola and Haynes 2004; Fueglistaler et al. 2005).

Temperature, specific humidity, and potential vorticity are interpolated from the ECMWF analyses to airmass locations (λ, ϕ, p) at time points along trajectories spaced at 6-h intervals. The interpolation is the same as used for the wind components in the trajectory integration. It is linear in time and the horizontal and a cubic-Lagrange interpolation in the vertical. The vertical velocity, η, is obtained in an identical manner to that in the ECMWF forecast model, and its boundary condition is employed in the trajectory integration. The ECMWF terrain-following η coordinate is used in all calculations.

b. Identifying the last condensation events

The "origin of humidity" in a dry air mass is set by the last condensation event experienced along its back trajectory. This occurs when the saturation specific humidity last equaled the "current specific humidity" at the arrival time. The global analysis is not a good estimate of "current q," owing to a lack of resolution of finescale features. As dry air masses approach the arrival grid, q interpolated from the analyses tends to increase as a result of numerical smoothing of the analysis model. Therefore, current q is estimated using the back trajectories as follows. Consider a parcel that at time $-\Delta t$ has specific humidity $q(-\Delta t)$, determined by interpolating the analyzed humidity to the air mass location at this time. If no mixing or water phase changes occur, the specific humidity is conserved along the trajectory. The condensation of water can be determined by comparing $q(-\Delta t)$ and the saturation specific humidity along the trajectory between time $t = -\Delta t$ and $t = 0$ and by assuming that instantaneous condensation occurs if a threshold relative humidity is exceeded. Throughout the paper the threshold used is 100%, but the sensitivity to this value is examined in section 2d.

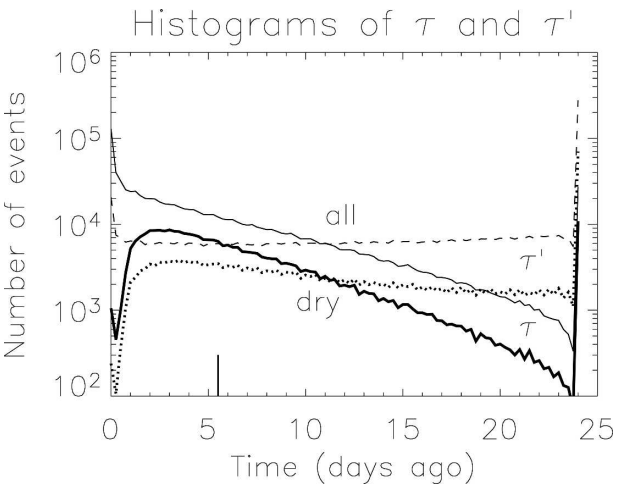

FIG. 1. Histogram of times since the last condensation event, τ (solid lines) and τ' (dashed lines), for all trajectories (thin lines) and for trajectories of air parcels that arrive dry (RH < 20%) at the release grid (bold lines). The median of the distribution of τ for dry air parcels, 5.5 days, is also marked.

Setting trajectory length Δt to a fixed value (24 days), the last condensation occurs at the time of minimum saturation specific humidity along the complete trajectory. This technique was used by Pierrehumbert and Roca (1998), Bonazzola and Haynes (2004), and Cau et al. (2005). The time when this occurs will be denoted as τ'. In this procedure it is implicitly assumed that remoistening does not occur through mixing or evaporation of condensate.

However, over such a long interval many air masses experience remoistening and subsequent condensation events that essentially reset the water vapor mixing ratio. This can be dealt with by repeating the search for the lowest saturation specific humidity, and recording it as a condensation event if it is below the airmass specific humidity $q(-\Delta t)$, for varying trajectory length $0 < \Delta t \leq 24$ days. The time since last condensation, τ, is defined as the shortest interval between arrival time and a condensation event setting humidity for any trajectory length. Clearly, if remoistening does not occur then $\tau = \tau'$, but generally $\tau < \tau'$.

The thin lines in Fig. 1 show the histograms of τ and τ' obtained considering all 892 800 back trajectories from the arrival grid throughout January 1993. The τ' histogram (dashed line) is almost flat, indicating that minimum saturation specific humidity along trajectories is equally likely to occur at any time, corresponding with the coldest temperature and lowest pressure. This

is not generally the case if the arrival region is narrowed to cover a specific pressure or latitude range. If remoistening is allowed, the τ histogram (solid line) exhibits an almost exponential shape. Its slope gives an exponential time scale of 7.0 days, which could be interpreted as the average time scale over which remoistening occurs following air masses, as represented by the 40-yr ECMWF Re-Analysis (ERA-40) system.

Henceforth the focus is on dry air masses that would tend to be associated with cloud-free air and the absence of convection, so that trajectories following the flow resolved in ERA-40 can be expected to be a good representation of the trajectories of air parcels. Following Cau et al. (2005), dry air masses are defined as those that have a relative humidity (RH) lower than 20% on the arrival grid. The RH is determined using temperature from the analysis at the arrival time (at the pressure level of the air mass) but the specific humidity inferred from the origin of a 1-day back trajectory $q(-1)$. This is because Cau et al. (2005) have shown that $q(-1)$ gives a better representation of dry layers observed by radiosondes than the humidity directly from the analysis $q(0)$ because the finite resolution of the analysis results in an unrealistic loss of finescale structure formed by differential advection. The humidity simulation correlates less well with observations when using longer trajectories because of the introduction of finescales that are not observed in exactly the same locations.

The bold lines in Fig. 1 show the histograms of τ and τ' obtained considering only back trajectories of air masses that are dry (RH $<$ 20%) on the arrival grid (288 020 trajectories). The τ histogram again exhibits an exponential fall for values greater than the median, marked by the vertical line (5.5 days). As before, the τ' histogram is much flatter (dotted line). However, for dry air masses the histograms tend to zero for short values of τ, since an air mass with an RH of 20% cannot have been saturated recently. The peak occurs at the short time of 2 days. It is worth noting that Sherwood et al. (2006) and Pierrehumbert et al. (2007) have recently proposed moisture distributions implied by a simple stochastic advection–condensation model, which could be used to explain the shape of these histograms.

c. Behavior of τ partitioned by arrival latitude and pressure

There is no reason to expect that the distribution of times since the last condensation will be the same throughout the troposphere. For dry air masses, it will largely depend on the rate of descent from a location with low $q_{\rm sat}$ to one where $q_{\rm sat}$ is high enough for RH to fall below 20%.

Figure 2 shows the τ histograms for all air masses and dry air masses, obtained for different latitude and pressure bands. The columns (labeled 1, 2, 3) correspond to air masses arriving in the southern subtropics (40°–15°S), Tropics (15°S–15°N), and northern subtropics (15°–40°N). The rows (labeled a, b, c) correspond to air masses arriving in the upper (425–175 hPa), mid- (675–425 hPa), and lower (975–675 hPa) troposphere. The number of trajectories that contribute to each plot is indicated in Fig. 5.

In all bands, the fall of the histogram for all trajectories, associated with remoistening, is mirrored in the histogram for dry air masses. However, as above, the dry airmass histogram must tend toward zero at short times. It is clear that the median τ for dry air masses is shortest for arrival in the upper troposphere (less than 5 days). It becomes slightly longer moving down to the lower troposphere in the subtropics, especially in the Southern Hemisphere (7 days). However, the increase in the median is much more obvious for dry air within the Tropics, reaching 11 days in the lower troposphere.

The histograms only have an exponential shape in the bands with a short median τ. However, all of them tail off substantially by 24 days. The spike at 24 days includes all the trajectories that do not experience condensation within the period. Clearly, a very small fraction of trajectories contribute to the spike. Regardless of the region, it is therefore possible to conclude that the chosen trajectory length of 24 days is sufficient to represent the humidity origin of the great majority of air masses.

Table 1 lists the percentage of air masses that do not experience condensation over 24-day trajectories (fourth column). As can be seen, the percentages are less than 6% everywhere except in the winter subtropics, where double this figure is found. The fifth column of Table 1 shows the percentage of trajectories originating above the tropopause (defined by the 2-PVU surface) 24 days before arrival. The percentages are generally much larger than those in the fourth column, indicating that remoistening occurs sometime over the 24-day trajectory and the humidity is reset in the troposphere. However, when the PV is examined along trajectories that do not experience any condensation, it is found that most of these air masses (especially in the lower troposphere) have a stratospheric origin (sixth column) and are too dry to reach saturation during the period.

d. Sensitivity to supersaturation with respect to ice

The results shown in all figures in this paper are obtained under the assumption that water vapor condenses when RH reaches 100%. However, it is well

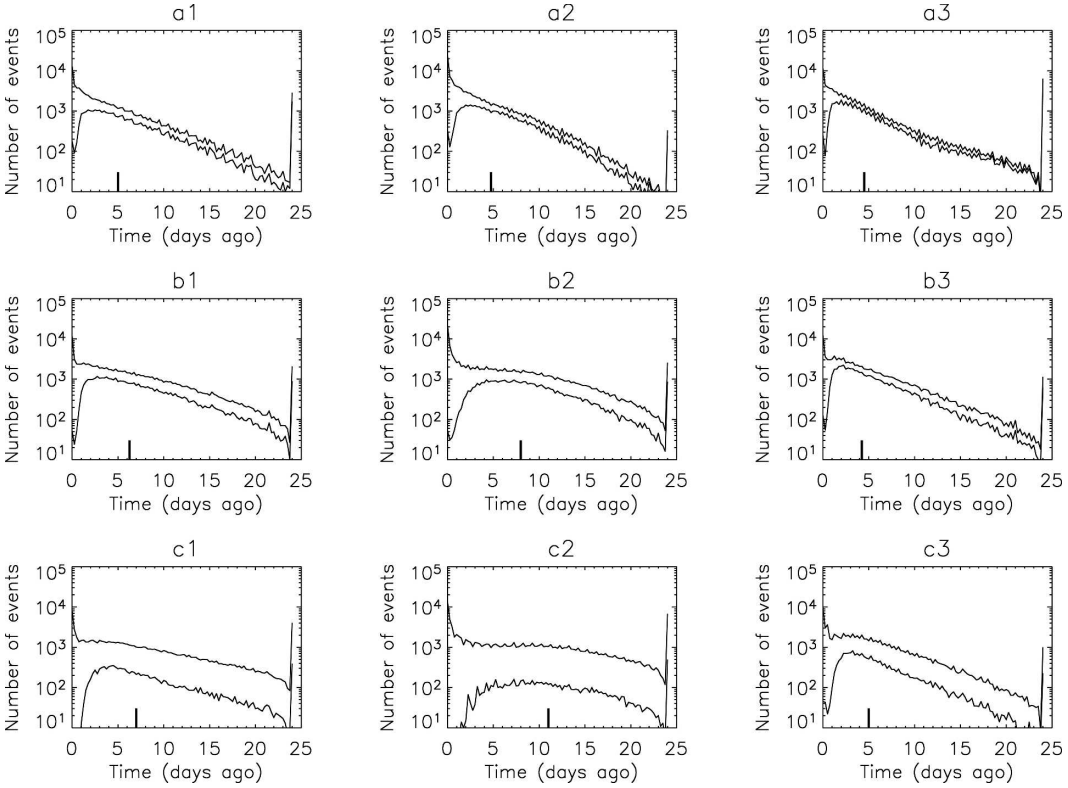

FIG. 2. Time since the last condensation (τ) for all air masses and dry air masses (lower curves), obtained for different latitude and pressure bands. The columns (labeled 1, 2, 3) correspond to air masses arriving in the latitude bands: 40°–15°S, 15°S–15°N, and 15°–40°N. The rows (labeled a, b, c) correspond to the pressure bands 175–425, 425–675, and 675–975 hPa.

known that air can often be supersaturated with respect to ice before condensation occurs. RH_i values as high as 170% have been observed near the tropical tropopause (Jensen et al. 2001), and over midlatitudes of the Northern Hemisphere large persistent supersaturation of up to 150% is a common occurrence (Gierens et al. 1999). High supersaturation occurs partly because of the long time scale for ice crystal growth.

The sensitivity of the results shown in this paper to supersaturation has been calculated by repeating them using several threshold values of RH_i. In the case of dry air masses, the median τ increases monotonically from 5.5 to 6.5 days when the threshold RH_i is varied from 105% to 180%. When considering all trajectories the median increases from 3.75 to 4.75 days. This is a small sensitivity, and Figs. 1, 2 are qualitatively unchanged

TABLE 1. Percentage of dry trajectories that do not experience condensation during the 24 days (NC, fourth column), partitioned into latitude and pressure bands as in Fig. 2. The fifth column shows the percentage of dry trajectories whose absolute PV exceeds 2 PVU at $\Delta t = -24$ days. The sixth column shows the percentage of dry trajectories with PV exceeding 2 PVU at $\Delta t = -24$ days out of the subset that did not experience condensation (NC).

Zone	Panel	Latitudes	P(NC)	P(PV > 2)	P(PV > 2 | NC)
All zones		40°S–40°N	3.8%	10.3%	60.8%
Upper troposphere (425–175 hPa)	a1	40°S–15°S	3.3%	4.2%	9.5%
	a2	15°S–15°N	0.4%	0.2%	4.9%
	a3	15°N–40°N	1.2%	8.0%	25.2%
Midtroposphere (675–425 hPa)	b1	40°S–15°S	2.2%	4.4%	24.0%
	b2	15°S–15°N	2.1%	2.1%	13.6%
	b3	15°N–40°N	1.2%	7.5%	42.1%
Lower troposphere (975–675 hPa)	c1	40°S–15°S	5.2%	11.3%	79.0%
	c2	15°S–15°N	0.2%	0.6%	42.4%
	c3	15°N–40°N	12.4%	19.5%	81.7%

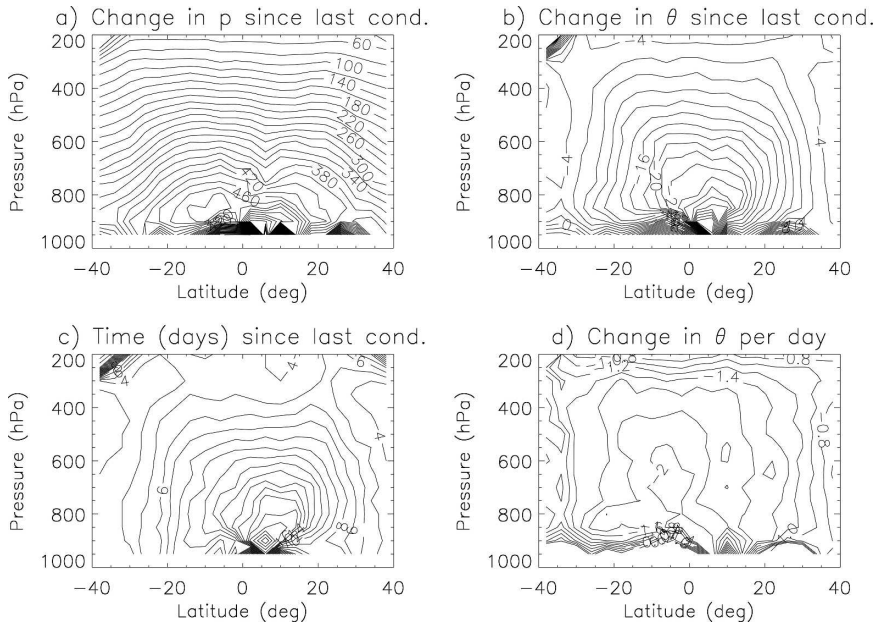

FIG. 3. Lagrangian means on arrival grid: (a) changes in pressure (hPa) since the last condensation along the trajectories, (b) changes of potential temperature (θ, K), (c) time since the last condensation (τ) in days, and (d) average material rate of change in θ since the last condensation ($\Delta\theta/\tau$) in K day^{-1}.

across the range of τ. Results reported later in the paper are also barely affected. For example, Figs. 3–8 are almost indistinguishable when the saturation RH with respect to ice is changed from 100% to 140%.

An argument for the insensitivity is that saturation vapor pressure falls so rapidly with temperature that q_{sat} falls with altitude even though the air pressure falls exponentially. An ascending air mass is likely to experience condensation at some point because q_{sat} falls so rapidly following the trajectory, and increasing the threshold RH only marginally delays the start of condensation. The time when condensation stops is set by the time of the temperature minimum, independent of the threshold RH, assuming that the condensation process is instantaneous. The median of τ increases with threshold RH_i because in a few cases air masses avoid condensation when $\text{RH}_i > 100\%$ only close to the highest point (coldest temperature) of the trajectory.

3. Net descent since last condensation

Figure 3a shows the change in pressure experienced since the last condensation, Δp, following air masses that arrive dry (RH $< 20\%$) at the analysis time. In some regions (e.g., the moist deep Tropics), the sample is small and does not represent the majority of air in that region. The values for trajectories arriving on the grid at different times and longitudes have been averaged at each point in the meridional cross section. Therefore the result is a Lagrangian mean. The Δp is remarkably invariant with latitude, showing only a slight decrease in net descent outside the Tropics. This is consistent with the distribution of q_{sat} being dominated by its vertical gradient. Greater descent is required to achieve RH less than 20% in the lower tro-

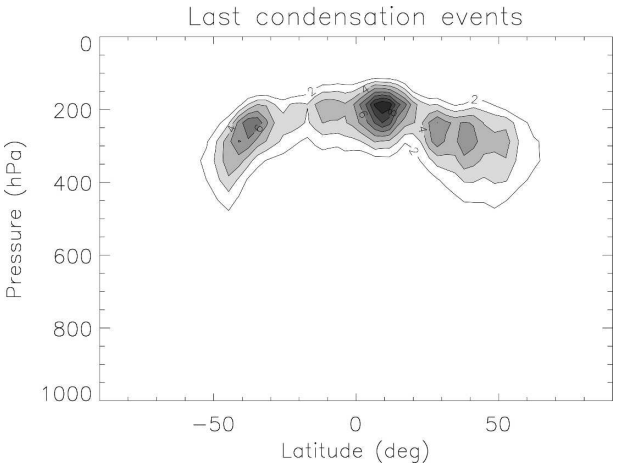

FIG. 4. Density of origin or number density of the last condensation events, summing events at all longitudes and times during January 1993 (277, 189 events), normalized so that integral of (1) over the atmosphere is unity. A value of 10 corresponds to 3625 trajectories experiencing condensation in a zonal box with $\Delta p =$ 50 hPa and $\Delta\mu = 2/45$ (4° lat near the equator).

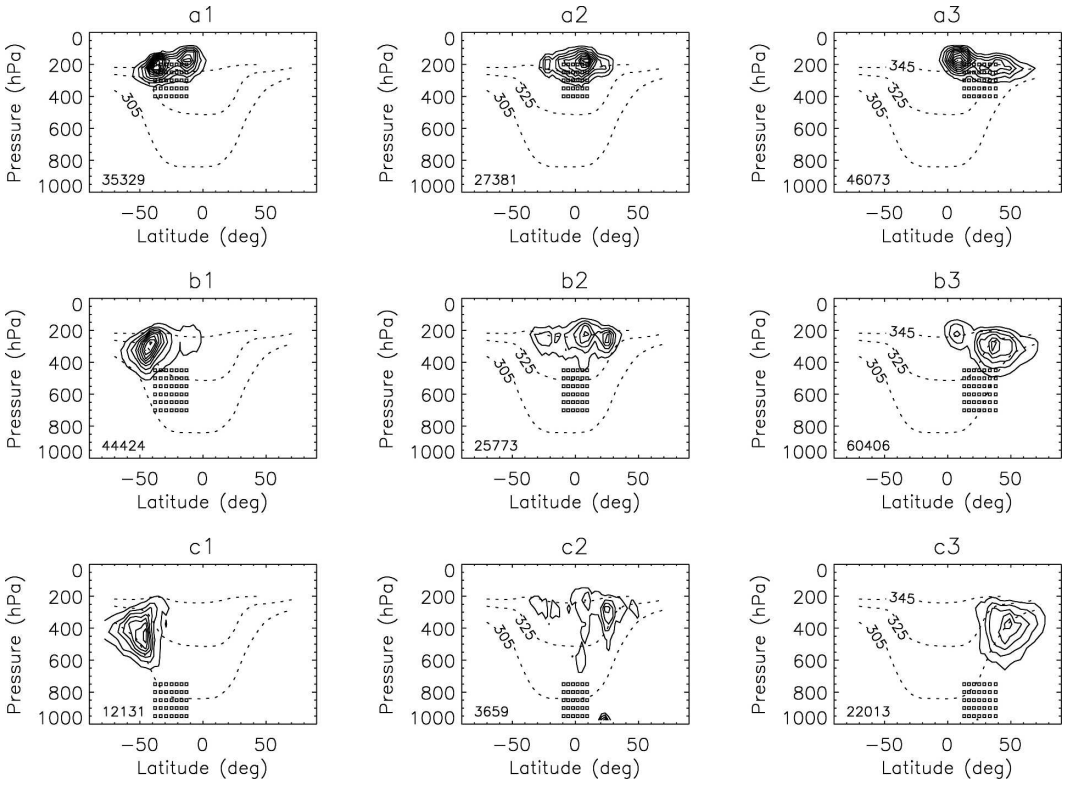

FIG. 5. Density of origin for dry air arriving at the grid points indicated in each box (same latitude and pressure bands as in Fig. 2). Dashed lines correspond to the monthly zonal mean isentropic levels at 305, 325, and 345 K. The number of dry trajectories arriving in each box is shown in the lower left corner.

posphere, resulting in the decrease in Δp with arrival altitude.

The mean time since the last condensation (Fig. 3c) is much lower poleward of 30° (only 5 days) than in the tropical lower troposphere where it exceeds 16 days. Since Δp hardly varies with latitude, this implies that the rate of descent is much faster into the subtropics than the Tropics.

The net change in potential temperature since the last condensation $\Delta\theta$ (Fig. 3b) resembles the distribution of mean τ. Their ratio gives the mean rate of change in potential temperature (or "heating") following air masses since the last condensation (Fig. 3d). The heating is everywhere negative and remarkably independent of arrival altitude, except close to the tropopause and the ground. It varies with the latitude of arrival between -0.8 K day^{-1} for the subtropics and -2.0 K day^{-1} near the equator, generally consistent with radiative cooling rates (Wallace and Hobbs 2006). This is quite a stringent test of the trajectory technique, since vertical motion is calculated in hybrid-pressure η coordinates from the continuity equation, which could result in errors in the evolution of potential temperature, even for adiabatic flow. Also, if the dry air masses and their time since the last condensation, diagnosed from the humidity field, were inconsistent with the vertical motion of the trajectory, one would expect to see potential temperature increases associated with the latent heat release for trajectories that pass through regions experiencing condensation in the ECMWF model.

In the deep Tropics the decrease in θ is sufficient to explain all the descent Δp. In other words, dry air masses can arise via slow diabatic descent across the stable stratification through the troposphere in the Tropics. The rate is consistent with radiative cooling. During the long time taken for descent, air masses travel large distances in the horizontal (section 5). In the subtropics, $\Delta\theta$ is not sufficient to account for the descent Δp, and a large component of descent is associated with equatorward motion and adiabatic descent down isentropic surfaces. Interestingly, τ is particularly high in the Tropics of the winter hemisphere, perhaps indicating that this region is to some extent isolated from air descending down isentropic surfaces from the extratropics, an idea supported by other analyses (B. J. Hoskins and P. Berrisford 2005, personal communication).

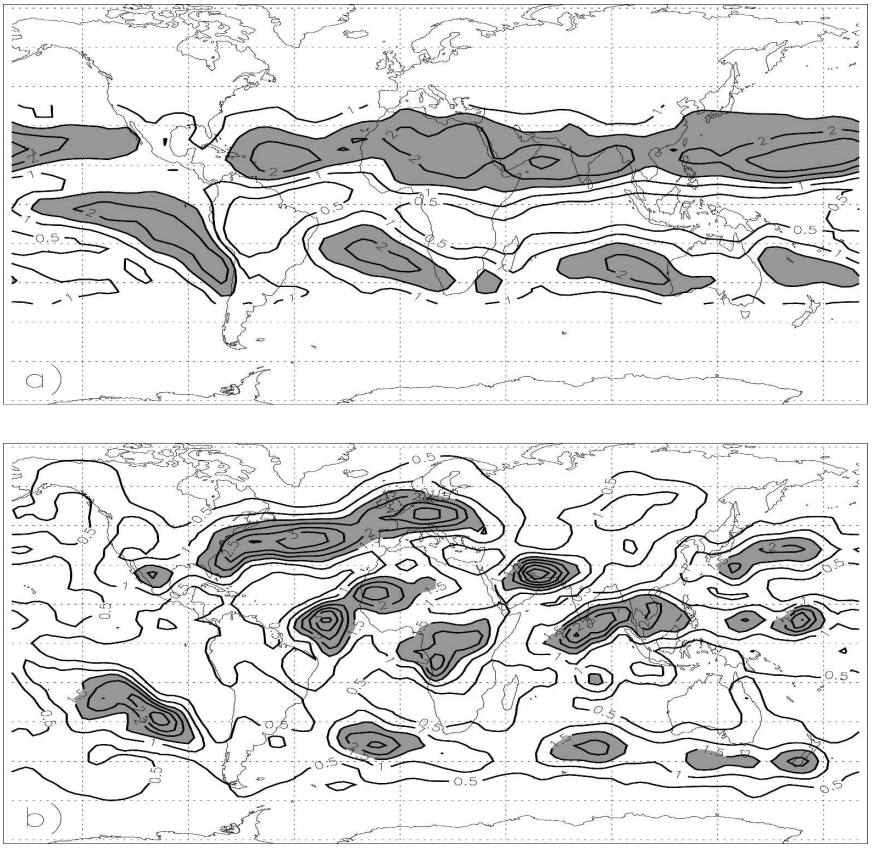

FIG. 6. Number density of (a) dry air masses (10 ster^{-1}) at all levels in the band 38°S–38°N determined from ERA-40 (288 020 events) and (b) last condensation events for the same dry air masses (277 189 experience condensation). The map extends from 75°S to 75°N and the density farther poleward is almost 0.

4. Lagrangian mean motion in the meridional plane

The meridional motion associated with slantwise descent is examined by finding the origins of dry air masses arriving in certain bands of latitude and altitude. Figure 4 shows the "density of origin" for all air masses that experience condensation and arrive dry (RH $<$ 20%) in the Tropics or subtropics. The origin of humidity is defined as the location where condensation last occurred and the density of origin is the number density of these condensation events in the meridional cross section. The number density is estimated over a regular grid in [μ, p] and therefore grid boxes contain equal mass. It is then normalized so that it integrates to unity over the mass of the atmosphere:

$$\int_0^{p_s} \int_{-1}^{1} \rho \, d\mu \, dp = 1. \tag{1}$$

Figure 4 shows that most condensation events occur in the upper troposphere, maximizing in the tropical winter hemisphere. There are substantial contributions from the extratropics of both hemispheres.

A partition of the arrival grid into three latitude and three pressure bands reveals the importance of the extratropics to lower-tropospheric humidity in the subtropics. Figure 5 shows the density of origin for the subdomains (grid shown on each panel). The Eulerian zonal- and time-mean potential temperatures are also shown by the dashed contours. It is clear that following condensation in the extratropics, air masses descend slightly steeper than the mean isentropic surfaces into the subtropics (Figs. 5c1,c3). Moving to the subtropical midtroposphere there is also a contribution of air from the tropical upper troposphere (Figs. 5b1,b3). This becomes the dominant contribution to dry air in the subtropical upper troposphere (Figs. 5a1,a3). A similar behavior was observed by Galewsky et al. (2005, their Fig. 10), who investigated the origin of dry air arriving at two reference pressure levels at latitude 20° using a different dataset and a different method. It is tempting to associate this tropical contribution with the Hadley

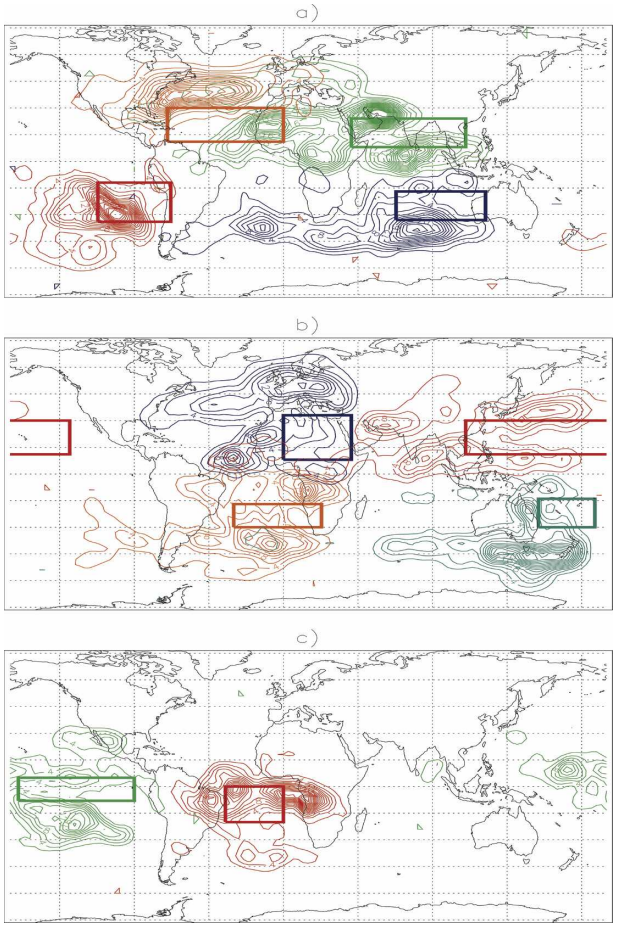

FIG. 7. Origin of air masses arriving in the boxed regions with RH < 20%. These boxes correspond to the regions with the most dry events (RH < 20%) in Fig. 6a and are listed in Table 2.

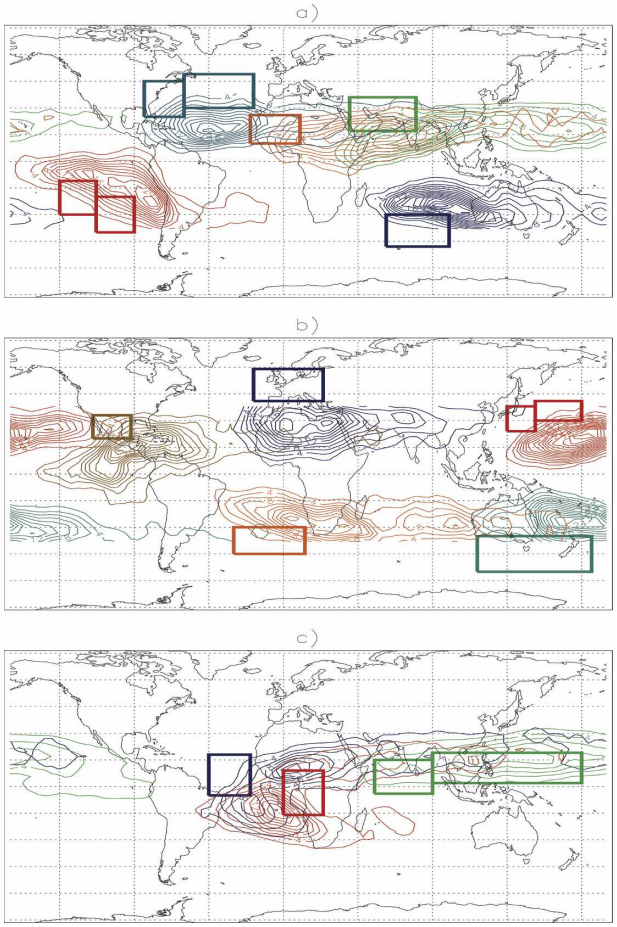

FIG. 8. Destination of air masses experiencing condensation in the boxed regions and arriving dry (RH < 20%) on the arrival grid. The boxes correspond to the maxima in density of origins (gray areas) in Fig. 6b and are listed in Table 2.

cell, although section 5 will show that zonal asymmetries in the subtropical jet play a major role.

Dry air at all levels within the Tropics mainly originates from the tropical upper troposphere, although there is an element of descent down isentropic surfaces from around 25°N and 25°S. As described in section 3, the diabatic descent is slow and consistent with radiative cooling rates.

5. Relating dry regions and preferred regions for condensation

a. Where does air in dry regions originate?

Dry air does not occur uniformly throughout the subtropics but exhibits a great deal of zonal asymmetry, particularly in the summer hemisphere where the driest air occurs within the subtropical anticyclones above the eastern side of the ocean basins.

Figure 6a shows the number density of dry air masses occurring throughout the atmospheric column during January 1993. As explained in section 2b, dry refers to RH less than 20% at the analysis time, where specific humidity is simulated using 1-day back trajectories rather than using analyzed q directly. In practice, the distribution obtained using analyzed RH is extremely similar. The number density is estimated using the method for kernel estimation on the sphere following Hodges (1996) and Jackson et al. (2001): a kernel function is centered on the location of each dry event and then the kernels are summed to create a density function that is smoothly varying. This removes discretization effects associated with accumulating counts within a fixed grid and bias associated with the varying area of grid boxes on the sphere. The smoothness of the density estimate is associated with the width of the kernels and the trade-off between retaining variance but reducing bias can be estimated by a maximum likelihood technique that selects the kernel width. Here the width

TABLE 2. Number of condensation events associated with each box in Figs. 7 and 8. The percentages at the bottom refer to the total number of trajectories that experience condensation (277 189), not to the total number of trajectories that are dry (288 020).

	Fig. 7		Fig. 8	
Panel	Region	Events	Region	Events
a	N Atlantic	18 757	N Atlantic	17 823
	S Asia	17 384	W Africa	7086
	SE Pacific	10 953	Middle East	8914
	SE Indian Ocean	9115	SE Pacific	12 974
			S Indian Ocean	6583
b	N Africa	15 218	W Europe	8847
	N Pacific	38 729	NW Pacific	6520
	S Atlantic	7430	Mexico	3189
	SW Pacific	7145	S Atlantic	7035
			Tasman Sea	9544
c	Tropical E Pacific	12 011	Tropical Atlantic	9013
	Tropical Atlantic	7021	Tropical Africa	8561
			Indo-Pacific	27 663
	Percentage of total	51.9%	Percentage of total	48.3%

of the kernels along a great circle is 636.5 km (corresponding to an arc width of 5.72°). The density is normalized so its integral over the solid angle of the globe equals unity. Therefore, it has units of ster^{-1}. The most striking zonal asymmetry in the relative humidity distribution is related to the southeast Pacific anticyclone and the dry air above the equatorial east Pacific. Dry air also occurs in the Tropics above the South Atlantic. In the Northern Hemisphere the band of dry air through the subtropics is only interrupted above Central America, Mexico, and the Caribbean.

Figure 6b shows the origin of dry air masses throughout the Tropics and subtropics. The clustering of preferred regions for condensation is striking. In the Southern Hemisphere there are four main centers on the upstream, poleward side of the subtropical anticyclones. Elsewhere the association between dry regions and regions of condensation cannot be determined directly from this plot. Dry air masses originate within the Atlantic and Pacific storm tracks, particularly at the upstream end. There are also clear centers over Europe, the Persian Gulf, Mexico, and West Africa. Within the Tropics, dry air originates from the central Atlantic, Africa, and a region stretching from the Indian Ocean to the west Pacific.

To study the stability of these features with respect to time, we also investigated another ENSO-neutral month (January 2005) and the ENSO-strong month of January 1998, and they both show the same set of features. While the two ENSO-neutral months closely agree in all density maxima with slightly different weights, January 1998 shows significant departure in the tropical region.

To identify the origins of air for each dry region, the trajectories are subsampled on the basis of their arrival location. Figure 7 outlines the selected regions with boxes of different colors and each density of origin is contoured in the corresponding color. The subtropical dry regions are staggered in Figs. 7a,b so that there is minimum overlap in their density of origins and the tropical dry regions are shown in Fig. 7c. Table 2 indicates the number of trajectories contributing to each dry region. Together, these regions contribute 51.9% of the dry air between 40°N and 40°S but only 36.9% of the surface area.

In the Southern Hemisphere, although the origin of each dry region lies mainly in the closest poleward and upstream region of condensation, as postulated from Fig. 6, some air originates from the next region of condensation to the west and is transported a great distance by the subtropical jet.

In the Northern Hemisphere, the subtropical dry band stretching across the Pacific (red, Fig. 7b) originates upstream from the Tropics, Pacific storm track, Persian Gulf, African, and even central Atlantic condensation regions, reflecting the speed of the winter subtropical jet. In contrast, the dry air over North Africa (black, Fig. 7b) has a strong component from much farther poleward, over Europe, as well as over the Atlantic storm track, West Africa, and the tropical Atlantic. Dry air over the subtropical North Atlantic originates almost exclusively from the Atlantic storm track (orange, Fig. 7a). The dry band from Arabia to Southeast Asia (green, Fig. 7a) mainly originates over the Persian Gulf, West Africa, tropical Africa, and the tropical Indian Ocean.

In the Tropics, the dry air over the east Pacific (green, Fig. 7c) condenses primarily as air from the southern subtropical jet enters the region of the subtropical high over the southeast Pacific. There is also a

significant contribution originating from Mexico and west of the date line in the Tropics. However, most of the air masses experiencing condensation over Peru and Ecuador end up in the South Pacific anticyclone (red, Fig. 7a), as shown previously by Salathé and Hartmann (1997, their Figs. 5, 6), rather than the tropical east Pacific (green, Fig. 7c). There is no evidence that the upward and downward branches of the Walker circulation over the tropical Pacific are connected by trajectories. On the other hand, the dry air over the tropical South Atlantic (red, Fig. 7c) originates both to the west (Amazon) and east (Congo). The ERA-40 climatology of streamfunction on the 330-K isentropic surface (Kållberg et al. 2005) indicates a stagnation point in this dry region and there is time-averaged convergence, more indicative of a divergent circulation.

b. Destination of dry air from preferred regions for condensation

The last section showed that most dry regions have contributions from several disconnected regions of origin. However, the converse link is clearer; the destinations of dry air from localized condensation regions tend to form smooth distributions with a single peak, usually in the closest dry region. Figure 8 shows the destination of air originating in selected areas identified as the maxima in the density of origin (Fig. 6b). The number density on the arrival grid is estimated using the same kernel width as for Fig. 6a. Table 2 shows the number of condensation events contributing to each highlighted region. Together these regions contribute 48.3% of the condensation events for air arriving dry between 40°N and 40°S.

In the Southern Hemisphere, the link between condensation near the subtropical jet and descent into the summer subtropical anticyclones is clear. Where the jet is strong, dry air can be carried a great distance before being captured by an anticyclone. The anticyclone in the southeast Pacific captures the most trajectories (see Table 2) and also brings dry air right into the tropical east Pacific.

In the Northern Hemisphere, links between isolated regions of condensation and dry air in the subtropics are much easier to identify than in Fig. 7. This is due to the capture of dry air from many regions of origin into the northern subtropical jet. Air experiencing the last condensation in the tropical upper troposphere is also drawn into the northern subtropical jet (Fig. 8c). In the zonal average this is a major contributor to the upper-tropospheric branch of the Hadley circulation.

Dry air in the Tropics originates from four main condensation regions: entering the southeast Pacific anticyclone from the southern subtropical jet, a similar but much weaker contribution from Mexico (see Table 2), and then condensation over the Congo and tropical Atlantic. These last two mainly contribute to dry air remaining in the upper troposphere over the tropical South Atlantic.

c. Transport mechanisms linking dry regions to their origins

Together Figs. 7 and 8 and the trajectories linking them (not shown) indicate four transport mechanisms between preferred regions of condensation and the dry regions of the Tropics and subtropics. These mechanisms are depicted schematically in Fig. 9. It is useful to compare them with the mean wind field in Kållberg et al. (2005).

1) EXTRATROPICAL BAROCLINIC WEATHER SYSTEMS

The schematic depicts the system-relative flow on an isentropic surface passing through the steering level of a baroclinic wave. Isentropic surfaces experiencing such flow range in potential temperature from 285 to 325 K. Descending air masses associated with extratropical weather systems in the storm tracks enter the subtropics rapidly with a large adiabatic component, descending sloping isentropic surfaces along branch A. Typically, the last condensation affecting such air masses occurs at a maximum in trajectory altitude (close to U) after the air masses have made a poleward excursion, ascending along branch D of the previous baroclinic system upstream. Air can also descend from the stratosphere along branch A, forming narrow intrusions of dry air with high potential vorticity.

The events are transient but the location of the storm track is persistent. The main regions of cyclogenesis are associated with a jet with increasing strength downstream. The North Atlantic (blue, Fig. 8a), northwest Pacific (red, Fig. 8b), South Atlantic (orange, Fig. 8b), and southern Indian Ocean (black, Fig. 8a) condensation regions fit this picture.

2) SUBTROPICAL ANTICYCLONES

The meridional component of the monthly mean tropospheric flow is most prominent around the subtropical anticyclones, especially in the summer hemisphere. The anticyclones have the greatest extent on isentropic surfaces that are close to the ground near the equator and slope toward the tropopause near the Poles. Kållberg et al. (2005) show the climatology of streamfunction on the 300-K potential temperature surface. The strongest subtropical anticyclone in DJF is found in the SE Pacific and air captured from the southern jet curves equatorward as it descends into the lower-level anticy-

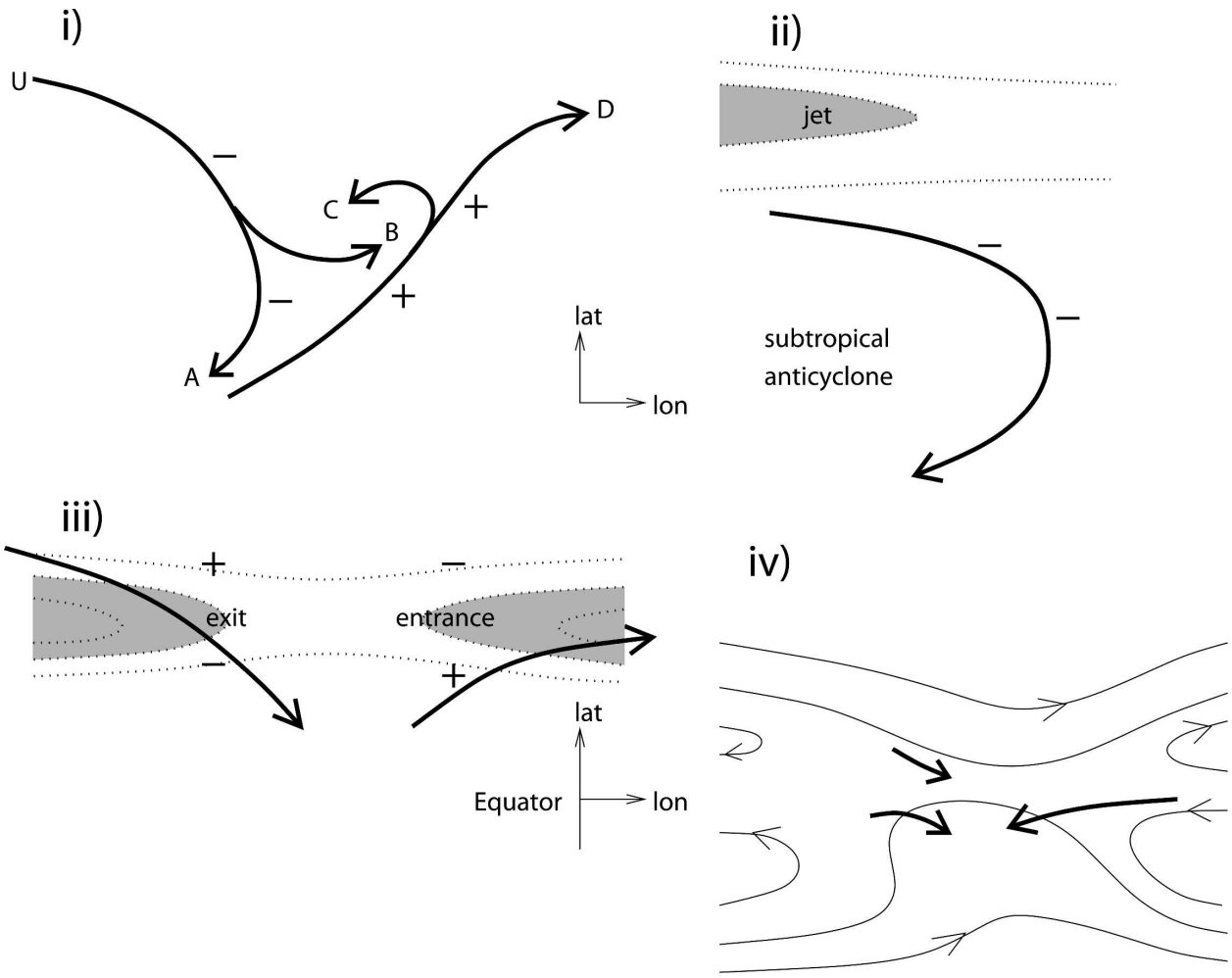

FIG. 9. Four transport processes linking dry air in the Tropics and subtropics to its origins. Arrows indicate typical trajectories. Dotted lines indicate isotachs of the time-average flow. Minus symbols mark descent and pluses mark ascent. (i) Extratropical baroclinic waves via their descending branch A; (ii) capture from the equatorial flank of the jet around subtropical anticyclones; and (iii) associated with a minimum in subtropical jet strength. Descent equatorward across the jet exit and ascent poleward into the jet entrance; and (iv) dry air converging near a stagnation region in the upper troposphere between regions of deep convection. Thin lines indicate the time-average streamfunction.

clone. It can then curve into the easterly trade winds as it approaches the equator (red, Fig. 8a). A similar but weaker process occurs in the Northern Hemisphere bringing dry air from Mexico into the equatorial east Pacific (brown, Fig. 8b). Since most air descending above the tropical East Pacific originates from the outside the Tropics, the ascending and descending branches of the Pacific Walker circulation are not linked by trajectories. Similar behavior could be expected during June–August (JJA) over the east Atlantic.

3) JET EXITS AND ENTRANCES

Where the subtropical jet decreases in strength along its axis in the seasonal average, there must be a secondary circulation across the jet exit with equatorward ageostrophic flow and descent on its equatorward flank. Extratropical air descends into the subtropics across this "jet exit." This mechanism is dominant for the Middle East (green, Fig. 8a) and southern Indian Ocean (black, Fig. 8a) condensation regions where the jet is strong but decreases with longitude in the upper troposphere [e.g., see the isotach climatology on the 250-hPa pressure level or 330-K isentropic level in Källberg et al. (2005)].

A complementary view is that minima in the jet are preferred locations for Rossby wave breaking, associated with equatorward intrusions of high potential vorticity air into the subtropics and Tropics. The flip side of this argument is that the time-average jet is weaker

where large amplitude breaking occurs regularly. Waugh and Polvani (2000) focused on events transporting high PV air directly into the Tropics (between 10°N and 10°S) and showed that these events are most frequent during Northern winter in the west Pacific sector where the subtropical jet decelerates and there are westerlies at the equator enabling a duct for Rossby wave propagation into the Tropics (see their Fig. 1). Such intrusions of stratospheric (high PV) air occur in the upper troposphere (above 330 K) and only rarely descend farther. However, on lower isentropic surfaces, the same breaking events transport dry air into the tropical lower troposphere from the extratropical upper troposphere, as described by Yoneyama and Parsons (1999). They will contribute to the set of trajectories experiencing condensation in the northwest Pacific (red, Fig. 8b).

In the jet entrance to the east of a minimum the secondary circulation is reversed and tropical upper-tropospheric air crosses poleward into the jet and then descends slowly at rates consistent with radiative cooling. This is prevalent for air condensing over the tropical Indian and West Pacific Oceans and to a lesser extent over Africa and the tropical Atlantic (Fig. 8c). This mechanism contributes to the zonally averaged Hadley circulation. Condensation within the jet entrances over West Africa (orange, Fig. 8a) and Mexico (brown, Fig. 8b) also contributes to dry air within the jet.

4) STAGNATION IN THE UPPER TROPOSPHERE

Dry air over the southern tropical Atlantic is centered on a region of weak winds in the time-averaged upper-tropospheric flow (around the 330-K isentropic surface; Kållberg et al. 2005), with air originating from the outflow from the convection in the Congo and Amazon regions (Fig. 8c). The time-average streamfunction is illustrated in the schematic, but the time-average velocity potential reveals steady horizontal convergence into this region from divergent regions associated with deep convection over the Congo and Amazon basins. The vertical and horizontal transport is slow in this case.

d. Regions experiencing a combination of mechanisms

Mechanism (i) involves large-amplitude transient waves on the midlatitude jet. In contrast, the other mechanisms invoke weak transient perturbations to the time-average flow, where trajectories are approximately parallel to streamlines but neighboring trajectories can separate rapidly near stagnation points (more precisely hyperbolic points). This scenario results in "chaotic advection" where the weak time variation of large-scale organizing wind structures results in the stretching and folding of air masses and the formation of long filaments in water vapor.

A combination of mechanisms (i) and (iii) affects air originating over Europe (black, Fig. 8b) and to a lesser extent the Tasman Sea (the longitudinal sector from Western Australia to New Zealand; green, Fig. 8b), which are both located at the end of a storm track and where the jet stream slows down in the midlatitudes. These condensation regions lie farther poleward than the others and are characterized by a strong equatorward component to the trajectories.

Furthermore, in the European sector the winter mean flow shows a split jet structure with the subtropical jet entrance situated to the south of the exit of the midlatitude jet. Descent is expected on the poleward flank of the subtropical jet entrance, reinforcing descent associated with being on the equatorward flank of the midlatitude jet exit, via mechanism (iii) (imagine shifting the jet exit in Fig. 9iii eastward and poleward until situated to the north of the jet entrance). At upper levels (on the 330-K isentropic surface), the subtropical jet entrance over West Africa lies above the eastern end of the Azores high (300 K). To some extent mechanism (ii) is also operative because of the time-average equatorward flow over the Sahara underneath the subtropical jet. Many trajectories descend southward across the midlatitude jet exit and slide farther southward under the subtropical jet in the lower-tropospheric anticyclonic circulation. During JJA, the subtropical jet in the upper troposphere becomes much weaker and shifts poleward over the Mediterranean Sea, but the Azores high becomes much stronger. Therefore, mechanism (ii) is expected to be a greater contributor in this region during summer.

6. Conclusions

The water vapor content in the dry regions of the tropical and subtropical troposphere is determined by their "origins," here defined as the last condensation event following airmass trajectories. These origins have been investigated using ERA-40 data for January 1993. Twenty-four-day back trajectories have been calculated and then the most recent condensation events identified. The method (section 2b) initializes humidity estimation by interpolating from the analyzed humidity at time $t = -\Delta t$ along a back trajectory. Then it is assumed that specific humidity is conserved following the air mass forward in time to $t = 0$ unless the relative humidity, calculated using temperature and pressure interpolated from the analyses to the trajectory points,

exceeds a threshold for condensation ($\geq$100%). Since remoistening and condensation may occur several times over 24-day trajectories, the search is repeated for all trajectory lengths $0 < \Delta t \leq 24$ days and the most recent condensation is assumed to set the humidity mixing ratio. It has been shown that 96% of air parcels experience condensation within 24 days and most of the remaining 4% originate in the stratosphere. Therefore, 24 days is a sufficient timespan to investigate the origin of humidity.

Lagrangian average linkages have been sought between dry air masses with relative humidity less than 20% at each analysis time and their origins. The net descent in terms of pressure increase is almost uniform with latitude, consistent with the dominance of vertical gradients in specific humidity associated with the temperature lapse rate and the Clausius–Clapeyron relation. However, the mean time taken for descent into the subtropics is only 5 days, whereas it exceeds 16 days into the tropical lower troposphere. The rate of decrease of potential temperature following the dry air masses varies with the latitude of arrival between -0.8 K day^{-1} for the subtropics and -2.0 K day^{-1} near the equator, consistent with radiative cooling. The results are remarkably insensitive to assumptions about the critical relative humidity with respect to ice required for condensation. Owing to the rapid drop of saturation specific humidity with height, most condensation events occur following a trajectory with whatever reasonable critical value is used.

Dry air masses in the subtropical lower troposphere mostly originate in the extratropics, descending more steeply than isentropic surfaces because of radiative cooling. Some dry air masses in the subtropical mid- to upper troposphere have origins in the tropical upper troposphere, which is consistent with the concept of a Hadley circulation when zonally averaged. However, zonal asymmetry is prevalent and the air originating in the tropical upper troposphere is typically captured in the northern subtropical jet where it is carried rapidly eastward. Dry air masses analyzed in the deep Tropics originate mainly in the tropical upper troposphere and descend at a rate consistent with radiative cooling.

The geographical origins of most of the dry air observed in the Tropics and the subtropics are clustered into distinct regions. Horizontal transport is important so that a dry region almost never overlaps with its humidity origin. Four transport processes are observed to operate: (i) descending air masses associated with extratropical weather systems in the storm tracks enter the subtropics rapidly with a large adiabatic component; (ii) the strongest subtropical anticyclone is found in the southeast Pacific, and air from the southern equatorial flank of the subtropical jet curves equatorward and then westward as it descends around the anticyclone toward the equator. Most of the air descending above the tropical east Pacific originates from outside the Tropics and the ascending and descending branches of the Pacific Walker circulation are not linked by trajectories; (iii) where the subtropical jet has a local minimum in strength, extratropical air descends across the jet exit into the subtropics and air from the tropical upper troposphere enters the jet where it speeds up and then descends slowly. A combination of processes (i) and (iii) affects air originating over western Europe and to a lesser extent the Tasman Sea, which are both located at the end of a storm track and where a midlatitude jet ends and the subtropical jet gains speed on the equatorward side; and (iv) dry air over the southern tropical Atlantic is centered on a stagnation region in the time-averaged upper-tropospheric flow, with dry air converging slowly from the convective outflow in the Congo and Amazon regions.

Data for only one January have been considered in this paper. However, this has yielded some 288 000 dry trajectories for study. By relating the results to aspects of the general circulation, four general mechanisms for the production of dry air in the Tropics and subtropics have been proposed. It would be of great interest to extend this study to span the entire ERA-40 period to examine seasonal variations and interannual variability.

Models used for climate change projections will represent in some form the four transport mechanisms associated with the origin of dry air (shown in Fig. 9). The ability of a model to represent these mechanisms (e.g., descent associated with midlatitude weather systems or fluctuations in the more steady jet structures) will have a bearing on its ability to represent the present-day humidity distribution. Furthermore, if the relative roles of the four transport mechanisms change in a future climate scenario, this will have a bearing on the simulated humidity distribution and water vapor feedback on the atmospheric response to radiative forcing. Sun and Lindzen (1993) have argued that in a warmer climate, deeper tropical convection might be expected to result in drier air exported from the tropical origins (Fig. 8c), opposing the water vapor feedback associated with higher global near-surface temperature and saturation vapor pressure. However, this transport pathway has the most effect on upper-tropospheric dryness, whereas lower-tropospheric humidity mainly originates from the extratropical upper troposphere. A fuller argument for changes to the humidity distribution and its feedbacks on temperature must involve a discussion of the changes in humidity origin for all transport mecha-

nisms, and the saturation vapor pressure at those origins, as the atmospheric climate evolves.

Acknowledgments. Piero Cau was funded throughout this research by the Natural Environment Research Council Grant NER/T/S/2001/00195 as part of their Clouds, Water Vapour and Climate thematic programme. John Methven is grateful for an Advanced Fellowship sponsored jointly by the Natural Environment Research Council and the Environment Agency.

REFERENCES

Bonazzola, M., and P. Haynes, 2004: A trajectory-based study of the tropical tropopause region. *J. Geophys. Res.,* **109,** D20112, doi:10.1029/2003JD004356.

Cau, P., J. Methven, and B. Hoskins, 2005: Representation of dry tropical layers and their origins in ERA-40 data. *J. Geophys. Res.,* **110,** D06110, doi:10.1029/2004JD004928.

Fueglistaler, S., M. Bonazzola, P. Haynes, and T. Peter, 2005: Stratospheric water vapor predicted from the Lagrangian temperature history of air entering the stratosphere in the tropics. *J. Geophys. Res.,* **110,** D08107, doi:10.1029/2004JD005516.

Galewsky, J., A. Sobel, and I. Held, 2005: Diagnosis of subtropical humidity dynamics using tracers of last saturation. *J. Atmos. Sci.,* **62,** 3353–3367.

Gierens, K., U. Schumann, M. Helten, H. Smit, and A. Marenco, 1999: A distribution law for relative humidity in the upper troposphere and lower stratosphere derived from three years of MOZAIC measurements. *Ann. Geophys.,* **17,** 1218–1226.

Hodges, K., 1996: Spherical nonparametric estimators applied to the UGAMP model integration for AMIP. *Mon. Wea. Rev.,* **124,** 2914–2932.

Holzer, M., and T. Hall, 2000: Transit-time and tracer-age distributions in geophysical flows. *J. Atmos. Sci.,* **57,** 3539–3558.

Houghton, J. T., Y. Ding, D. J. Griggs, M. Noguer, P. J. van der Linden, X. Dai, K. Maskell, and C. A. Johnson, Eds., 2001: *Climate Change 2001: The Scientific Basis.* Cambridge University Press, 881 pp.

Jackson, D., J. Methven, and V. Pope, 2001: Transport in the low latitude tropopause zone diagnosed using particle trajectories. *J. Atmos. Sci.,* **58,** 173–192.

Jensen, E., L. Pfister, A. Ackerman, A. Tabazadeh, and O. Toon, 2001: A conceptual model of the dehydration of air due to freeze-drying by optically thin, laminar cirrus rising slowly across the tropical tropopause. *J. Geophys. Res.,* **106,** 17 237–17 252.

Kållberg, P., P. Berrisford, B. Hoskins, A. Simmons, S. Uppala, S. Lamy-Thépaut, and R. Hine, 2005: ERA-40 Atlas. ECMWF Re-Analysis Project Rep. 19, 191 pp. [Available online at http://www.ecmwf.int/research/era/ERA-40_Atlas/docs/index.html.]

Methven, J., 1997: Offline trajectories: Calculation and accuracy. UGAMP Tech. Rep. 44, University of Reading, Reading, United Kingdom, 18 pp.

——, and B. Hoskins, 1999: The advection of high resolution tracers by low resolution winds. *J. Atmos. Sci.,* **56,** 3262–3285.

——, S. Arnold, F. O'Connor, H. Barjat, K. Dewey, J. Kent, and N. Brough, 2003: Estimating photochemically produced ozone throughout a domain using flight data and a Lagrangian model. *J. Geophys. Res.,* **108,** 4271, doi:10.1029/2002JD002955.

Pierrehumbert, R., 1999: Subtropical water vapor as a mediator of rapid global climate change. *Mechanisms of Global Climate Change at Millennial Time Scales, Geophys. Monogr.,* Vol. 112, Amer. Geophys. Union, 339–361.

——, and R. Roca, 1998: Evidence for control of Atlantic subtropical humidity by large scale advection. *Geophys. Res. Lett.,* **25,** 4537–4540.

——, H. Brogniez, and R. Roca, 2007: On the relative humidity of the Earth's atmosphere. *The Global Circulation of the Atmosphere: Phenomena, Theory, Challenges,* T. Schneider and A. Sobel, Eds., Princeton University Press, in press.

Salathé, E., and D. Hartmann, 1997: A trajectory analysis of tropical upper-tropospheric moisture and convection. *J. Climate,* **10,** 2533–2547.

Sherwood, S. C., 1996: Maintenance of the free-tropospheric tropical water vapor distribution. Part II: Simulation by large-scale advection. *J. Climate,* **9,** 2919–2934.

——, E. R. Kursinski, and W. G. Read, 2006: A distribution law for free-tropospheric relative humidity. *J. Climate,* **19,** 6267–6277.

Soden, B., and R. Fu, 1995: A satellite analysis of deep convection, upper-tropospheric humidity, and greenhouse effect. *J. Climate,* **8,** 2333–2351.

Sun, D.-Z., and R. Lindzen, 1993: Distribution of tropical tropospheric water vapor. *J. Atmos. Sci.,* **50,** 1643–1660.

Wallace, J., and P. Hobbs, 2006: *Atmospheric Science: An Introductory Survey.* 2d ed. Academic Press, 483 pp.

Waugh, D., and L. Polvani, 2000: Climatology of intrusions into the tropical upper troposphere. *Geophys. Res. Lett.,* **27,** 3857–3860.

Yoneyama, K., and D. Parsons, 1999: A proposed mechanism for the intrusion of dry air into the tropical western Pacific region. *J. Atmos. Sci.,* **56,** 1524–1546.